

Extremum Seeking Control of a Robotic Ankle-Foot Orthosis Targeting the Soleus Muscle Activation During Walking

Evan Tulsky¹, Nicholas Rubino¹, Jade Carter¹, Aiko K. Thompson², Victor H. Duenas¹

Abstract—Stroke survivors experience muscle weakness and low weight-bearing capacity that impair their walking. The activation of the plantarflexor muscles is diminished following a stroke, which degrades propulsion and balance. Powered exoskeletons can improve gait capacity and restore impaired muscle activity. However, a technical barrier exists to generate systematic control methods to predictably and safely perturb the paretic leg using a wearable device to characterize the plantarflexors' muscle output for gait training. In this paper, a closed-loop robust controller is designed to impose an ankle joint rotation (i.e., a kinematic perturbation) in the mid-late stance phase to target the soleus muscle using a powered cable-driven ankle-foot orthosis. The goal is to generate soleus muscle activity increments throughout a gait experiment by applying ankle perturbations. This ability to modulate plantarflexor activity can be used in future conditioning studies to improve push-off and propulsion during walking. However, the optimal perturbation magnitude for each participant is unknown. Hence, online adaptation of the ankle perturbation is well-motivated to modulate the soleus response measured using surface electromyography (EMG). An extremum seeking controller (ESC) is implemented in real-time to compute the ankle perturbation magnitude (i.e., dorsiflexion angle) exploiting the soleus EMG response from the previous perturbed step to maximize the soleus response in the next perturbed step. A Lyapunov-based stability analysis is used to guarantee exponential kinematic tracking of the ankle perturbation objective.

Index Terms—Extremum seeking control; ankle exoskeleton; nonlinear systems

I. INTRODUCTION

Stroke survivors experience gait and sensory deficits, weak voluntary muscle activations, low weight-bearing capacity, and loss of balance that negatively interfere with activities of daily living [1]. Restoring gait function is a priority for stroke survivors [2]. Powered exoskeletons and therapeutic interventions can improve range of motion, restore gait function, and improve endurance [3], [4]. However, typical robotic-assisted approaches cannot ensure people post-stroke will retain gait benefits once the assistance provided by the device is removed. Furthermore, stroke survivors can

*Research reported in this publication was supported in part by the National Science Foundation under Grant No. 2218913 and by pilot funding from the National Institutes of Health National Center of Neuromodulation for Rehabilitation, the National Center for Complementary and Integrative Health, the National Institute on Deafness and Other Communication Disorders, and the National Institute of Neurological Disorders and Stroke; NIH/NICHD Grant Number P2CHD086844 which was awarded to the Medical University of South Carolina. The contents are solely the responsibility of the authors and do not necessarily represent the official views of the NSF, NIH or NICHD.

¹Department of Mechanical and Aerospace Engineering, Syracuse University, Syracuse NY 13244, USA. ²Medical University of South Carolina, Charleston SC 26425, USA. Email: {ertulsky, narubino, jcarter19, vhduenas}@syr.edu {thompsai}@musc.edu

develop a reliance on robotic assistive devices that can result in misuse of the paretic leg [5]. Hence, it is well-motivated to develop gait training approaches to encourage the human to produce voluntary muscle contraction in the paretic leg. However, a technical challenge is to integrate wearable devices and their controllers during these types of gait training strategies.

The ankle joint and plantarflexors are critical for walking because they store mechanical energy throughout the stance phase leading to propulsive push-off [6], [7]. However, muscle activation patterns and propulsion are diminished in the paretic leg after a stroke. In the mid-late stance phase, load-sensing Ib afferents are active and reinforce ankle extensor activity (i.e., soleus muscle loading response) that triggers propulsion and force generation [8]. However, after a stroke, the soleus muscle is not loaded correctly, which diminishes paretic plantarflexor activity and limits gait speed. Targeting and increasing the activity of the soleus muscle during walking can facilitate training and promote lasting gait benefits [9] (e.g., natural soleus activity and increased propulsion) without developing a dependence on an assistive device.

Exoskeletons can impose gait patterns that aim to replicate normal activation of muscles [10], however, the effectiveness of such approaches to induce lasting gait benefits has not been established. Open-loop perturbations applied to the ankle joint have been demonstrated to yield increased excitation in ankle flexor and extensor muscles [8]. Alternatively, a backstepping controller with an integral control input was developed to target the soleus muscle using surface electromyography (EMG) to track a predetermined excitation level [11]. However, it is unknown how to determine the optimal perturbation magnitude during walking to accommodate for the specific characteristics of the human. Hence, an online adaptive strategy is well-motivated to compute the perturbation magnitude based on the muscle responses during walking.

Extremum seeking control (ESC) is an adaptive-based method that leverages an unknown input-output map with a local or global extremum to implement online optimization of a nonlinear system [12]. The classical ESC architecture uses a dither signal to inject excitation and explore the neighborhood around a setpoint to find the extremum. One of the main advantages of ESC is that knowledge of the cost function and the input-output map does not need to be known [12]. In the context of human-robot interaction, ESC has been used to control lower-limb prostheses [13], maximize the human's power output in an exercise machine [14],

with functional electrical stimulation-induced cycling [15], and to minimize muscular effort in an ankle exoskeleton [16].

This paper exploits the ESC as a real-time adaptive method to compute the ankle kinematic perturbation magnitude (i.e., joint angle deviation from the natural ankle kinematics) to characterize the unknown ankle angle-soleus muscle activation map (i.e., the relationship between the perturbation input and the muscle output).

In this paper, an ESC algorithm leveraging the architecture in [12], [14], [17] is developed to compute the ankle perturbation angle using a motorized ankle-foot orthosis and soleus EMG measurements. The objective is to perturb the ankle joint using the device to generate increments in soleus muscle responses (i.e., maximize the muscle activity) during walking. The capacity to modulate the soleus muscle responses using the device despite differences across participants (e.g., differences in muscle force production, joint kinematics, etc.) will be exploited in subsequent studies for gait training. A closed-loop robust feedback controller is designed to track the computed perturbation by the ESC algorithm during the mid-late stance phase of walking. A piecewise continuous switching signal is developed to activate the perturbation controller using ground reaction force measurements and the ankle angular velocity to stop the perturbation. A Lyapunov-based stability analysis is developed to ensure global exponential tracking of the perturbation trajectory.

II. CONTROL DEVELOPMENT

Fig. 1 depicts the block diagram of the closed-loop ankle perturbation controller. The participant wears a robotic ankle-foot orthosis during walking. The soleus muscle activity (denoted S after signal processing) and ankle angular position and velocity q, \dot{q} are measurable. An ESC algorithm is implemented to generate the ankle perturbation trajectory and a nonlinear robust controller is designed to track the perturbation, and thus, apply the perturbation about the ankle joint using the device. The ESC algorithm and robust tracking controller are developed in the following subsections.

A. Extremum Seeking Control for Ankle Perturbation Trajectory Generation

To apply perturbations about the ankle joint, a kinematic perturbation trajectory $q_d : \mathbb{R}_{\geq t_0} \rightarrow \mathbb{R}$ can be generated using ESC such that $q_d \in \mathcal{L}_\infty$ and $q_d \rightarrow \hat{q}_d^*$, where \hat{q}_d^* is an unknown optimal perturbation magnitude that maximizes the participant's soleus muscle response during walking (i.e., generate the largest increment in muscle response with respect to the baseline muscle activity) and $t_0 \in \mathbb{R}_{>0}$ denotes the initial time. The perturbation trajectory is obtained by imposing a deviation from the natural ankle kinematics within the mid-late stance phase of walking. A Bézier curve $q_b : \mathbb{R}_{\geq t_0} \rightarrow \mathbb{R}$ is designed to depart from the current natural ankle joint trajectory q (i.e., the actual ankle position), impose the perturbation (i.e., an ankle dorsiflexion), and then connect back to the natural ankle trajectory in real-time. However, the perturbation magnitude $Q_d \in \mathbb{R}_{>0}$ (i.e.,

the peak dorsiflexion) that yields predictable soleus muscle activity increments is unknown. Hence, the ESC algorithm computes a perturbation magnitude trajectory $Q_d : \mathbb{R}_{\geq t_0} \rightarrow \mathbb{R}$ that is used to calculate \tilde{Q}_d . The ESC algorithm and the Bézier curve are then used to generate the perturbation trajectory q_d for the tracking objective as illustrated in the block diagram in Fig.1.

The measurable soleus muscle response $S : \mathcal{Q} \times \mathbb{R} \rightarrow \mathbb{R}_{\geq 0}$ can be modeled as [18], [19]

$$S(q, \dot{q}) = s_1 + s_2 q(t) + s_3 \dot{q}(t), \quad (1)$$

which is measurable using EMG, $q : \mathbb{R}_{\geq t_0} \rightarrow \mathcal{Q}$ denotes the measurable ankle joint angular position, $\dot{q} : \mathbb{R}_{\geq t_0} \rightarrow \mathbb{R}$ denotes the measurable angular velocity, $\mathcal{Q} \subseteq \mathbb{R}$ is the set of ankle angles, and $s_1, s_2, s_3 \in \mathbb{R}_{>0}$ are uncertain positive constants. The objective of the ESC algorithm is to yield increments of the steady state value of soleus muscle response S due to the applied ankle perturbations without requiring the knowledge of \hat{q}_d^* . The only assumption is that \hat{q}_d^* exists such that each participant can evoke a maximum soleus response during walking. Inspired by ESC algorithms [14], [15], [17] that leverage dither signals to aid with convergence to a neighborhood of the extremum, a saturated extremum-seeking algorithm is developed to generate the ankle dorsiflexion (perturbation) magnitude profile $Q_d : \mathbb{R}_{\geq t_0} \rightarrow \mathbb{R}$ as

$$\begin{aligned} w &= -(k_h^2 \nu + k_h \text{sat}_\beta(S)), \\ \dot{\hat{\theta}} &= -k_\theta w \sin(\omega q), \\ \dot{\nu} &= -(k_h \nu + \text{sat}_\beta(S)), \\ Q_d &= \hat{\theta} + (\alpha_p - \frac{k_d}{\alpha_p} w) \sin(\omega q), \end{aligned} \quad (2)$$

which leverages S from the previous perturbed step to generate the perturbation trajectory for the next perturbed step computed as $q_d(t) \triangleq \tilde{Q}_d q_b(t)$, where $\tilde{Q}_d \triangleq \text{med}(Q_d)$ is the median of Q_d . The median is a robust measure with respect to the peak-to-peak variability. In the ESC algorithm in (2), $\alpha_p \in \mathbb{R}_{>0}$ denotes a positive constant amplitude of the dither signal, $\omega \in \mathbb{R}_{>0}$ denotes the frequency of the dither, $k_d, k_\theta, k_h \in \mathbb{R}_{>0}$ denote positive constant parameters, $\hat{\theta}, \nu, w : \mathbb{R}_{\geq t_0} \rightarrow \mathbb{R}$ denote auxiliary signals, and $\text{sat}_\beta(\cdot)$ denotes the saturation function defined as

$$\text{sat}_\beta(\cdot) \triangleq \begin{cases} \cdot & \text{for } |\cdot| \leq \beta \\ \text{sgn}(\cdot)\beta & \text{for } |\cdot| > \beta \end{cases}, \quad (3)$$

where $\beta \in \mathbb{R}$ is a saturation limit and $\text{sgn}(\cdot) : \mathbb{R} \rightarrow [-1, 1]$ is the signum function. The saturation function is integrated in the ESC algorithm in (2) to ensure Q_d is bounded, and hence, q_d is bounded since the Bézier curve q_b is bounded by design. The ESC algorithm in (2) replaces the typical time-based dither signal in classical ESC with a time-invariant dither (i.e., state-dependent) as in [20] to adapt the joint perturbation trajectory using the ankle angle q within the perturbation region in the stance phase of walking. The state-dependent time-invariant dither signal proportionally

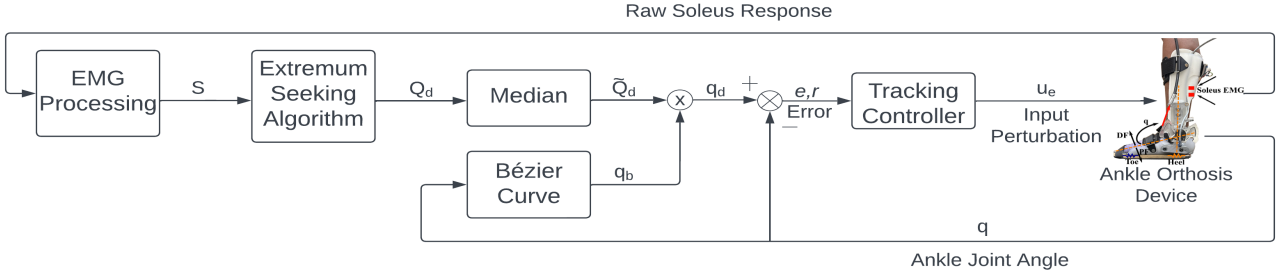


Fig. 1. Block diagram of the human-robot system. The participant wears the ankle orthosis during walking. The ankle joint angle and velocity, q , \dot{q} , and the soleus muscle activity (EMG) are collected. The soleus EMG is rectified and low-pass filtered to obtain S , which is the input to the ESC algorithm. ESC computes the perturbation angle trajectory Q_d for the next perturbed step using the soleus EMG data from the previous perturbed step. The median of the trajectory Q_d is denoted as \bar{Q}_d . Concurrently, a Bézier curve q_b is implemented to generate the deviation from the actual ankle angle trajectory q to apply the joint perturbation and then smoothly connect to the natural ankle trajectory (outside of the perturbation region). The perturbation trajectory q_d used for the tracking objective is obtained as $q_d = \bar{Q}_d q_b$. The tracking controller u_e applies the perturbation input using the tracking errors e, r .

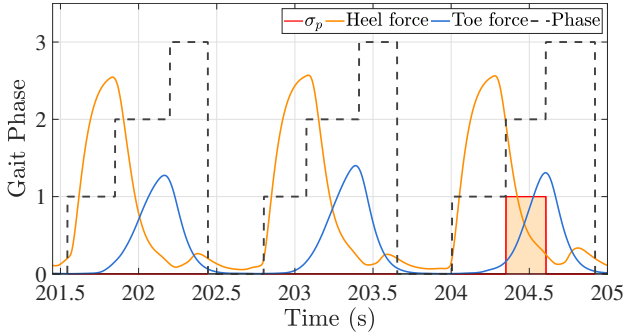


Fig. 2. The gait phase detection (dashed gray) computed using the heel (orange) and toe (blue) ground reaction forces and ankle angular velocity (not shown) is depicted for three consecutive step cycles. The switching signal σ_p (red) determines when perturbations are applied. The ankle perturbation is not applied in the first two steps ($\sigma_p = 0$). Then, the kinematic perturbation is applied in the third step during mid-late stance phase ($\sigma_p = 1$). The phases transition between $phase = 0$ (swing), $phase = 1$ (heel strike and early stance), $phase = 2$ (perturbation region in mid-late stance), and $phase = 3$ (stop perturbation in terminal stance), which ensures the perturbation is halted prior to the start of the swing phase. The perturbation region is denoted by $\sigma_p = 1$ depicted by the shaded orange region in the third step.

updates the ESC based on the evolution of the stance phase and the ankle kinematics. A time-dependent dither signal is not implemented because the ESC algorithm and tracking controller are only switched on in the mid-late stance phase and switched off elsewhere. In this way, the ESC is active within the soleus muscle loading phase in the step cycle.

B. Dynamic Model

The single degree-of-freedom ankle-joint muscle-tendon and powered orthosis system can be modeled with the following dynamics

$$J\ddot{q}(t) + f(q(t), \dot{q}(t)) + G(q(t)) + d(t) = \tau(t), \quad (4)$$

where $J \in \mathbb{R}_{>0}$ is an uncertain positive constant denoting the combined inertia of the overall ankle-foot orthosis and joint-muscle system; $\ddot{q} : \mathbb{R}_{\geq t_0} \rightarrow \mathbb{R}$ denotes the unmeasurable ankle angular acceleration; the nonlinear function $f : \mathcal{Q} \times \mathbb{R} \rightarrow \mathbb{R}$ denotes the elasticity due to the ankle stiffness and

the viscous effects due to damping in the musculotendon complex as derived in [21], [22]; $G : \mathcal{Q} \rightarrow \mathbb{R}$ denotes the effects of gravity; and $d : \mathbb{R}_{\geq t_0} \rightarrow \mathbb{R}$ denotes the external disturbances and the biological torque from the human. The torque applied by the electric motor about the ankle joint is denoted by $\tau : \mathbb{R}_{\geq t_0} \rightarrow \mathbb{R}$ and is defined as

$$\tau(t) \triangleq \sigma_p B_e u_e(t), \quad (5)$$

where $u_e : \mathbb{R}_{\geq t_0} \rightarrow \mathbb{R}$ is the motor current control input designed subsequently, $B_e \in \mathbb{R}_{>0}$ is a known positive torque constant, and $\sigma_p \in \{0, 1\}$ is a piecewise constant switching signal developed to apply an ankle joint perturbation per step cycle within the mid-late stance phase of walking (i.e., the perturbation region). The switching signal is defined as $\sigma_p = 1$ within the perturbation region and $\sigma_p = 0$ outside of the perturbation region to stop perturbing the ankle joint and thus, interfering with natural ankle kinematics. A gait phase detection algorithm is implemented to compute the switching signal σ_p using heel and toe ground reaction forces to determine the heel strike and define the perturbation phase. The ankle angular velocity \dot{q} is used to determine when to stop the perturbation phase. The perturbation phase ends when the ankle joint reaches peak dorsiflexion such that $\dot{q} > 0$. Fig. 2 depicts the transition of gait phases, the toe and heel forces and an example of a perturbation region (i.e., the shaded region when $\sigma_p = 1$).

The following assumption and properties are exploited the subsequent control design and analysis.

Assumption 1. *The additive disturbance d is bounded as $|d| \leq \zeta_d$, where $\zeta_d \in \mathbb{R}_{>0}$ is a known positive constant.*

Property 1. *$|f(q, \dot{q})| \leq c_{f1} + c_{f2}|\dot{q}|$, where $c_{f1}, c_{f2} \in \mathbb{R}_{>0}$ are known constants [23].*

Property 2. *$|G(q)| \leq \bar{g}$, where $\bar{g} \in \mathbb{R}_{>0}$ is a known constant [24, Ch. 3].*

C. Ankle Perturbation Tracking Controller

To quantify the kinematic tracking objective, a measurable angular joint position error $e : \mathbb{R}_{\geq t_0} \rightarrow \mathbb{R}$ and an auxiliary

filtered tracking error $r : \mathbb{R}_{\geq t_0} \rightarrow \mathbb{R}$ are defined as

$$e(t) = q_d(t) - q(t), \quad (6)$$

$$r(t) = \dot{e}(t) + \alpha e(t), \quad (7)$$

where $\alpha \in \mathbb{R}_{>0}$ is a selectable constant control gain and $q_d : \mathbb{R}_{\geq t_0} \rightarrow \mathbb{R}$ is the bounded ankle perturbation trajectory.

The open-loop error system is obtained by taking the time derivative of (7), pre-multiplying it by J , substituting for (4), (6) and (7), and performing algebraic manipulation as

$$J\dot{r} = J\ddot{q}_d + f(q, \dot{q}) + G(q) + d - \tau + J\alpha r - J\alpha^2 e. \quad (8)$$

Segregating terms that can be upper bounded by a positive constant and a state-dependent function, respectively, the following auxiliary signals $N_d : \mathbb{R}_{\geq t_0} \rightarrow \mathbb{R}$ and $\tilde{N} : \mathbb{R}_{\geq t_0} \rightarrow \mathbb{R}$ are defined as

$$N_d \triangleq d + J\ddot{q}_d + f(q_d, \dot{q}_d) + G(q_d), \quad (9)$$

$$\begin{aligned} \tilde{N} \triangleq & f(q, \dot{q}) - f(q_d, \dot{q}_d) + G(q) - G(q_d) + J\alpha r \\ & - J\alpha^2 e + e, \end{aligned} \quad (10)$$

where the desired dynamics $\tau_d(q_d, \dot{q}_d) : \mathbb{R}_{\geq t_0} \rightarrow \mathbb{R} \triangleq f(q_d, \dot{q}_d) + G(q_d)$ were added and subtracted in (9) and (10), respectively, to generate an upperbound of (10) using the mean value theorem. The auxiliary signal in (9) can be upper bounded as $|N_d| \leq \xi_d$ leveraging Assumption 1 and the fact that $\tau_d \in \mathcal{L}_\infty$, where $\xi_d \in \mathbb{R}_{>0}$ is a known positive constant. The auxiliary signal in (10) can be upperbounded as $|\tilde{N}| \leq \varrho(\|z\|)\|z\|$, where $z : \mathbb{R}_{\geq t_0} \rightarrow \mathbb{R}^2$ is defined as $z \triangleq [e \ r]^T$, and $\varrho : \mathbb{R} \rightarrow \mathbb{R}$ is a known positive, non-decreasing, radially unbounded function.

Given the open-loop error system in (8), the control input is designed as

$$u_e \triangleq k_1 r + k_2 \text{sgn}(r) + k_3 \varrho^2(\|z\|)r, \quad (11)$$

where $k_1, k_2, k_3 \in \mathbb{R}_{>0}$ are selectable positive gain constants. The motor control input in (11) includes a feedback term, a high-frequency term to compensate for the auxiliary term in (9) that is upper bounded by a constant, and a nonlinear damping term to compensate for the auxiliary signal in (10) that is upper bounded by a state-dependent function. The closed-loop kinematic error system is obtained by substituting (5), (9), (10), and (11) when $\sigma_p = 1$ into (8) as

$$J\dot{r} = \tilde{N} + N_d - e - B_e \left(k_1 r + k_2 \text{sgn}(r) + k_3 \varrho^2(\|z\|)r \right). \quad (12)$$

III. STABILITY ANALYSIS

The stability of the closed-loop ankle kinematic controller to impose joint perturbations during the mid-late stance phase can be examined using the following theorem.

Theorem 1. *The controller in (11) ensures global exponential joint kinematic tracking within the perturbation region, i.e., for $\sigma_p = 1$, in the sense that*

$$\|z(t)\| \leq \sqrt{\frac{\lambda_2}{\lambda_1}} \|z(t_0)\| e^{-\frac{\delta}{4\lambda_2}(t-t_0)}, \quad (13)$$

provided the following sufficient gain conditions are satisfied

$$k_2 \geq \frac{\xi_d}{B_e}, \delta \triangleq \min\{\alpha, k_1 B_e\} > \frac{1}{2k_3 B_e}. \quad (14)$$

Proof. Let $V : \mathbb{R}^2 \times \mathbb{R}_{\geq t_0} \rightarrow \mathbb{R}$ be a positive definite, radially unbounded, continuously differentiable Lyapunov function candidate defined as

$$V \triangleq \frac{1}{2}e^2 + \frac{1}{2}Jr^2. \quad (15)$$

The function in (15) satisfies the following inequalities

$$\lambda_1 \|z\|^2 \leq V(z, t) \leq \lambda_2 \|z\|^2, \quad (16)$$

where $\lambda_1 \triangleq \min(\frac{1}{2}, \underline{J})$ and $\lambda_2 \triangleq \max(\frac{1}{2}, \bar{J})$, where $\underline{J}, \bar{J} \in \mathbb{R}_{>0}$ are positive constant bounds of the system's inertia J . Let $z(t)$ be a Filippov solution to the differential inclusion $\dot{z} \in K[h](z)$, where $K[h](\cdot)$ is defined as in [25], and h is defined by using (7) and (12) as $h \triangleq [h_1 \ h_2]$, where

$$h_1 \triangleq r - \alpha e,$$

$$h_2 \triangleq \frac{1}{J} \{ \tilde{N} + N_d - e - B_e(k_1 r + k_2 \text{sgn}(r) + k_3 \varrho^2(\|z\|)r) \}.$$

The control input in (11) has the signum function; hence, the time derivative of (15) exists almost everywhere (a.e.), i.e., for almost all t . Based on [26, Lemma 2], $\dot{V}(z, t) \overset{a.e.}{\in} \hat{V}(z, t)$, where \hat{V} is the generalized time derivative of (15) along the Filippov trajectories of $\dot{z} = h(z)$ and is defined in [26] as $\hat{V} \triangleq \bigcap_{\xi \in \partial V} \xi^T K \begin{bmatrix} \dot{e} & \dot{r} & 1 \end{bmatrix}^T (e, r, t)$, where $\partial V(z, t)$ is the generalized gradient of V at (z, t) . Since $V(z, t)$ is continuously differentiable in z , $\partial V = \{\nabla V\}$, $\hat{V} \overset{a.e.}{\subset} [e, Jr]K \begin{bmatrix} \dot{e} & \dot{r} \end{bmatrix}^T$. Therefore, after substituting (7) and (12), canceling common terms, the generalized time derivative of (15) can be expressed as

$$\begin{aligned} \dot{V} \overset{a.e.}{\subset} & -\alpha e^2 + r(\tilde{N} + N_d \\ & - B_e(k_1 r + k_2 \text{sgn}(r) + k_3 \varrho^2(\|z\|)r)), \end{aligned} \quad (17)$$

where $K[\text{sgn}(r)] = SGN(r)$ such that $SGN(r) = 1$ if $r > 0$, $[-1, 1]$ if $r = 0$, and -1 if $r < 0$. Substituting the upper bounds of (9) and (10), the previous expression can be upperbounded as

$$\begin{aligned} \dot{V} \overset{a.e.}{\leq} & -\alpha e^2 - k_1 B_e r^2 - (k_2 B_e - \xi_d)|r| \\ & + \varrho(\|z\|)\|z\||r| - k_3 B_e \varrho^2(\|z\|)r^2. \end{aligned} \quad (18)$$

By completing the squares for the last two terms in the previous inequality, (18) can be rewritten as

$$\dot{V} \overset{a.e.}{\leq} -\alpha e^2 - k_1 B_e r^2 - (k_2 B_e - \xi_d)|r| + \frac{1}{4k_3 B_e} \|z\|^2. \quad (19)$$

Provided the gain conditions in (14) are satisfied, the inequality in (19) can be further upper bounded as

$$\dot{V} \overset{a.e.}{\leq} -\frac{\delta}{2} \|z\|^2 - \left(\frac{\delta}{2} - \frac{1}{4k_3 B_e} \right) \|z\|^2. \quad (20)$$

By invoking [26, Corollary 2], $|e|, |r| \rightarrow 0$ as $t \rightarrow \infty$. Using the inequalities in (16) and (20) and solving the differential inequality yields (13). Since $V > 0$ and $\dot{V} \overset{a.e.}{\leq} 0$, $V \in \mathcal{L}_\infty$;

hence, $e, r \in \mathcal{L}_\infty$, which implies that $z \in \mathcal{L}_\infty$, and thus $u_e \in \mathcal{L}_\infty$ in (11) and $\tau \in \mathcal{L}_\infty$ in (5). Since $e, r \in \mathcal{L}_\infty$, then $\dot{e} \in \mathcal{L}_\infty$ from (7), and hence $q, \dot{q} \in \mathcal{L}_\infty$, which implies $\ddot{q} \in \mathcal{L}_\infty$ from (12). ■

IV. APPARATUS

The apparatus consists of a powered, wearable ankle-foot orthosis that is customizable to various foot sizes. Fig. 3 depicts the wearable ankle device. Straps are utilized around the foot and shank to maintain alignment with the user's ankle joint. The wearable orthosis has a mechanism to apply unilateral joint perturbations to the left ankle using cable-driven actuation as in [8], [27]. The device is connected to a separate actuation unit with a brushless 24 VDC electric motor (Maxon International Ltd.) to apply torque inputs about the ankle joint. An optical encoder (US Digital) is mounted on the orthosis to measure the ankle joint angular position q and velocity \dot{q} . The heel and toe reaction forces are measured using force sensitive resistors (FlexiForceA401), which are placed within the sole of the foot orthosis. EMG data of the soleus muscle is collected using two 0.875×1.375 inch electrode pads (13-NEURO PLUS A10041-60) placed one inch apart along the center line of the lower leg below the head of the gastrocnemius. The surface electrodes are connected to a Bortec AMT-8 amplifier to amplify and send the EMG data to the data acquisition board (QPIDE, Quanser) connected to a desktop computer (Windows 10 OS) running a real-time target sampled at 1 kHz (QUARC 2.6, Quanser) using MATLAB/Simulink 2018a (Mathworks, Inc.). A modified treadmill (NordicTrack T7.5S) is used for the walking experiments and a closed-loop controller is implemented to keep the treadmill belt at the desired constant walking speed. For safety purposes, the participants have access to an emergency stop button and software stop conditions are implemented to limit the amount of motor current compliant with hardware limits.

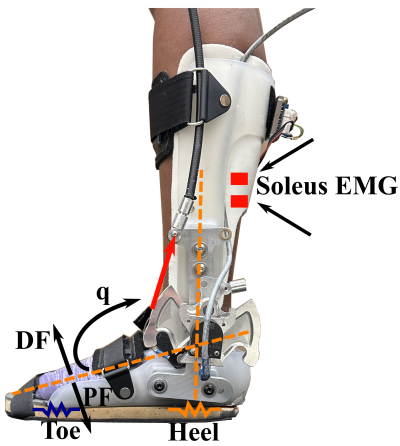


Fig. 3. The wearable orthosis is connected to a cable-driven system actuated by an electric motor to apply torque inputs about the ankle joint using the controller in (11). The cable applies tension as shown using the red arrow to rotate the ankle joint q . The perturbations are applied as dorsiflexions (DF) or upward rotations of the ankle. The toe and heel ground reaction forces are collected using force sensitive resistors. EMG measurements are collected on the soleus muscle.

V. CONCLUSION

In this paper, a closed-loop robust controller was developed to track a perturbation trajectory using a customized powered ankle-foot orthosis with a cable-driven mechanism. The wearable orthosis is used to apply ankle joint perturbations within the mid-late stance phase of walking. The perturbation trajectory was updated by a state-dependent ESC algorithm to generate increments in the soleus muscle activity with respect to the baseline muscle activation while walking. The ankle dorsiflexions applied to evoke increments in the activity of the soleus muscle will be used for gait training in people post-stroke. The robust controller included feedback terms to compensate for the effects of exogenous disturbances and upper bounds of the uncertainties in the dynamic model. Future work includes the implementation of the closed-loop controller and ESC algorithm in stroke survivors during walking.

REFERENCES

- [1] V. Weerdesteyn, M. De Niet, H. J. Van Duijnhoven, *et al.*, "Falls in individuals with stroke," *J. Rehabil. Res. Dev.*, vol. 45, no. 8, pp. 1195–1214, 2008.
- [2] A. Pollock, B. St George, M. Fenton, *et al.*, "Top 10 research priorities relating to life after stroke - consensus from stroke survivors, caregivers, and health professionals," *Int. J. Stroke*, vol. 9, no. 3, pp. 313–320, 2014.
- [3] L. Marchal-Crespo and D. J. Reinkensmeyer, "Review of control strategies for robotic movement training after neurologic injury," *J. Neuroeng. Rehabil.*, vol. 6, no. 1, 2009.
- [4] T. G. Hornby, D. S. Reisman, I. G. Ward, *et al.*, "Clinical practice guideline to improve locomotor function following chronic stroke, incomplete spinal cord injury, and brain injury," *J. Neurol. Phys. Ther.*, vol. 44, no. 1, pp. 49–100, Jan. 2020.
- [5] A. L. Hall, C. L. Peterson, S. A. Kautz, *et al.*, "Relationships between muscle contributions to walking subtasks and functional walking status in persons with post-stroke hemiparesis," *Clin. Biomech.*, vol. 26, no. 5, pp. 509–515, 2011.
- [6] D. A. Winter, *Biomechanics and Motor Control of Human Movement*. New York: Wiley, 1990.
- [7] E. J. Rouse, H. Lee, and H. I. Krebs, "Summary of human ankle mechanical impedance during walking," *IEEE J. Transl. Eng. Health Med.*, vol. 4, pp. 1–7, 2016.
- [8] N. Mazzaro, M. J. Grey, and T. Sinkjær, "Contribution of afferent feedback to the soleus muscle activity during human locomotion," *J. Neurophysiol.*, vol. 93, no. 1, pp. 167–177, 2005.
- [9] A. K. Thompson, C. R. Gill, W. Feng, *et al.*, "Operant down-conditioning of the soleus h-reflex in people after stroke," *Front. Rehabilit. Sci.*, vol. 3, 2022.
- [10] M. Gandolla, E. Guanziroli, A. D. Angelo, *et al.*, "Automatic setting procedure for exoskeleton-assisted overground gait: Proof of concept on stroke population," *Front. Neurorob.*, vol. 12, no. 10, Mar. 2018.
- [11] N. Rubino, E. Lawler, J. Casas, *et al.*, "Backstepping control of a motorized ankle orthosis targeting the soleus muscle during walking," *IFAC-PapersOnLine*, vol. 56, no. 2, pp. 4484–4489, 2023, 22nd IFAC World Congress.
- [12] M. Krstic and H.-H. Wang, "Stability of extremum seeking feedback for general nonlinear dynamic systems," *Automatica*, vol. 36, no. 4, pp. 595–601, Apr. 2000.

- [13] S. Kumar, A. Mohammadi, D. Quintero, *et al.*, “Extremum seeking control for model-free auto-tuning of powered prosthetic legs,” *IEEE Trans. Control Syst. Tech.*, vol. 28, no. 6, pp. 2120–2135, 2020.
- [14] X. T. Zhang, D. M. Dawson, W. E. Dixon, *et al.*, “Extremum seeking nonlinear controllers for a human exercise machine,” *IEEE Trans. Mechatron.*, vol. 11, pp. 233–240, 2006.
- [15] V. H. Duenas, C. A. Cousin, C. A. Rouse, *et al.*, “Extremum seeking control for power tracking via functional electrical stimulation,” *IFAC-PapersOnLine*, vol. 51, no. 34, pp. 164–169, 2019, 2nd IFAC Conference on Cyber-Physical and Human Systems CPHS 2018.
- [16] S. Kumar, M. R. Zwall, E. A. Bolívar-Nieto, *et al.*, “Extremum seeking control for stiffness auto-tuning of a quasi-passive ankle exoskeleton,” *IEEE Rob. Autom. Letters*, vol. 5, no. 3, pp. 4604–4611, 2020.
- [17] M. Guay, “A perturbation-based proportional integral extremum-seeking control approach,” *IEEE Trans. Autom. Cont.*, vol. 61, no. 11, pp. 3370–3381, 2016.
- [18] J. Yang, R. Stein, and K. James, “Contribution of peripheral afferents to the activation of the soleus muscle during walking in humans,” *Exp. Brain Res.*, vol. 87, pp. 679–687, 1991.
- [19] G. L. Gottlieb and G. C. Agarwal, “Response to sudden torques about ankle in man: Myotatic reflex,” *J. Neurophysiol.*, vol. 42, no. 1, pp. 91–106, 1979.
- [20] S. Kumar, A. Mohammadi, R. D. Gregg, *et al.*, “Limit Cycle Minimization by Time-Invariant Extremum Seeking Control,” *Proc. Amer. Control Conf.*, pp. 2359–2365, 2019.
- [21] R. Riener, F. Ferrarin, E. E. Pavan, *et al.*, “Patient-driven control of FES-supported standing up and sitting down: Experimental results,” *IEEE Trans. Rehabil. Eng.*, vol. 8, no. 4, pp. 523–529, 2000.
- [22] T. Schauer, N. O. Negård, F. Previdi, *et al.*, “Online identification and nonlinear control of the electrically stimulated quadriceps muscle,” *Control Eng. Pract.*, vol. 13, no. 9, pp. 1207–1219, Sep. 2005.
- [23] C. Chang, J. Casas, and V. H. Duenas, “Closed-loop kinematic and indirect force control of a cable-driven knee exoskeleton: A lyapunov-based switched systems approach,” *IEEE Open J. Control Syst.*, vol. 2, pp. 171–184, 2023.
- [24] F. L. Lewis, D. M. Dawson, and C. T. Abdallah, *Robot Manipulator Control*. 2003, p. 638.
- [25] A. F. Filippov, “Differential equations with discontinuous right-hand side,” in *Fifteen papers on differential equations*, ser. American Mathematical Society Translations - Series 2, vol. 42, American Mathematical Society, 1964, pp. 199–231.
- [26] N. Fischer, R. Kamalapurkar, and W. E. Dixon, “LaSalle-Yoshizawa corollaries for nonsmooth systems,” *IEEE Trans. Autom. Control*, vol. 58, no. 9, pp. 2333–2338, Sep. 2013.
- [27] J. B. Andersen and T. Sinkjaer, “Mobile ankle and knee perturbator,” *IEEE Trans. Biomed. Eng.*, vol. 50, no. 10, pp. 1208–1211, 2003.